

Designing quantum experiments with a genetic algorithm

Rosanna Nichols,¹ Lana Mineh,^{2,3} Jesús Rubio,⁴ Jonathan C. F. Matthews,⁵ and Paul A. Knott^{1,*}

¹*Centre for the Mathematics and Theoretical Physics of Quantum Non-Equilibrium Systems (CQNE), School of Mathematical Sciences, University of Nottingham, University Park, Nottingham, NG7 2RD, UK.*

²*Quantum Engineering Centre for Doctoral Training, University of Bristol, Bristol, UK.*

³*Now at: School of Mathematics, University of Bristol, UK.*

⁴*Department of Physics and Astronomy, University of Sussex, Brighton, BN1 9QH, UK.*

⁵*Quantum Engineering Technology Labs, H. H. Wills Physics Laboratory and Department of Electrical & Electronic Engineering, University of Bristol, BS8 1FD, UK.*

(Dated: April 19, 2022)

We introduce a genetic algorithm that designs quantum optics experiments for engineering quantum states with specific properties. Our algorithm is powerful and flexible, and can easily be modified to find methods of engineering states for a range of applications. Here we focus on quantum metrology. First, we consider the noise-free case, and use the algorithm to find quantum states with a large quantum Fisher information (QFI). We find methods, which only involve experimental elements that are available with current technology, for engineering quantum states with up to a 100-fold improvement over the best classical state, and a 20-fold improvement over the optimal Gaussian state. Such states are a superposition of the vacuum with a large number of photons (around 80), and can hence be seen as Schrödinger-cat-like states. We then apply the two most dominant noise sources in our setting – photon loss and imperfect heralding – and use the algorithm to find quantum states that still improve over the optimal Gaussian state with realistic levels of noise. This will open up experimental and technological work in using exotic non-Gaussian states for quantum-enhanced phase measurements. Finally, we use the Bayesian mean square error to look beyond the regime of validity of the QFI, finding quantum states with precision enhancements over the alternatives even when the experiment operates in the regime of limited data.

Engineering quantum states with specific properties plays a part in all experiments and technologies in quantum physics. But designing optimal experiments to engineer such states can be challenging, in part due to the counter-intuitive nature of the theory. This has prompted a number of recent works allocating the task of experiment-design to artificial intelligence and machine learning [1–5]. Many of the computer-designed experiments have surpassed the best human-designed alternatives.

Building on this approach, we introduce a genetic algorithm, named Ada (or AdaQuantum) [8], that designs quantum optics experiments to produce quantum states with the required properties. The algorithm is flexible and modifiable, so that researchers with a range of requirements and available quantum-optics equipment can use it to design and optimise their experiments, as well as facilitating theoretical research in quantum state engineering and experimental design. In addition, the algorithm has a powerful computational engine, so that it efficiently and effectively searches for the optimal experimental designs in a given setting, and can allow for truncations of the Hilbert space up to 170 photons, enabling even more exotic states to be found. A selection of the experiments designed by Ada are shown schematically in Fig. 5.

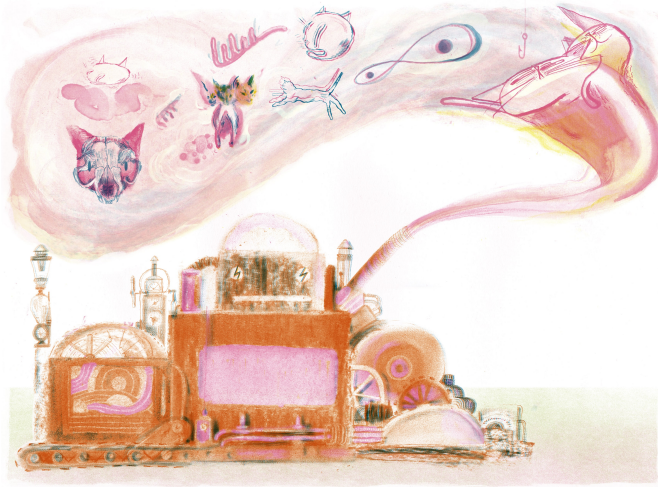
To run Ada we must specify two things: first, we specify the *toolbox* of equipment that is available to con-

struct our experiment, or more specifically, which quantum states, operations, and measurements we would like Ada to optimise over. Second, we must specify a fitness function, which allows us to quantify *how good* the quantum state outputted by Ada is for our purposes. In principle, any fitness function that takes as input a quantum state, and outputs a real number, can be used. Given this, Ada then performs an automated search to find arrangements and parameter settings of the experiential equipment that produce a state that maximises (or minimises) the fitness function. The flexibility built into Ada means that different fitness functions can easily be implemented, such as the fidelity with useful quantum states such as Schrödinger-cat states or states used in optical quantum computation [7]; or measures of entanglement, coherence, non-classicality, and so on. An artist’s impression of Ada is shown in Fig. 1, which depicts the algorithm producing a wide range of quantum states.

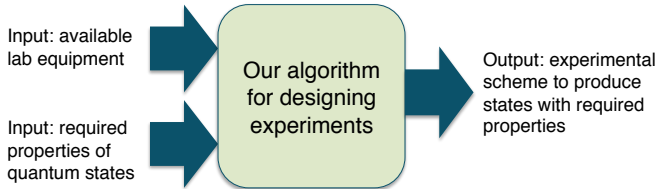
In this work we focus on fitness functions relevant to the field of quantum metrology. We first consider noise-free experiments, and use as our fitness function the quantum Fisher information (QFI) of the (pure) output state. The QFI allows us to quantify how precisely a given state can measure a phase shift in an interferometer – a valuable fitness function for optical quantum metrology [9, 10]. Next, we apply the two most dominant noise sources in our quantum optics setting – photon loss at the output, and imperfect heralding measurements – and use the mixed state QFI as our fitness function.

The third fitness function that we optimise is the Bayesian mean square error (BMSE). Although the QFI plays a crucial role in quantum metrology, its use requires

* Contact email address: Paul.Knott@Nottingham.ac.uk



(a)



(b)

FIG. 1. a) An artist's impression of our algorithm, Ada, which designs experiments for engineering quantum states. The algorithm is designed for flexibility, and can produce a wide range of quantum states; the illustration depicts, among others, the production of a Schrödinger-cat state, a three-headed cat state [6], and a GKP state [7]. Most relevant for this paper is the quantum Fisher information, also depicted here (subtly). Artwork by Joseph Namara Hollis. b) A flow chart illustrating the overall structure and usage of our algorithm for designing quantum experiments.

a number of assumptions that are not always fulfilled in experiments. For example, it often assumes that a large number of repetitions has taken place and that certain prior information was available [11–14]. The BMSE, on the other hand, factors in and allows us to control both of these explicitly, and thus gives a reliable measure of the phase-measuring capability of a given state in realistic experimental settings [15].

Our main results obtained by Ada are threefold: First, in the noiseless case we find a number of methods of producing quantum states with QFIs up to 20 times larger than the optimal Gaussian state, which amounts to a 100-fold improvement over the best classical state. We show that these states can be thought of as Schrödinger-cat-like states, as they contain superpositions of the vacuum with a large numbers of photons (around 80). Second, we find methods of producing states that can still beat the optimal Gaussian state, even when realistic levels of

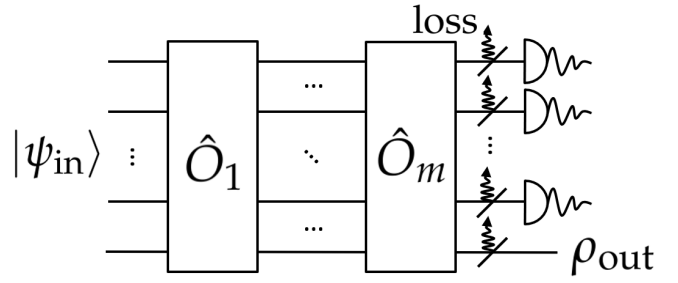


FIG. 2. The generic blueprint for the quantum optics experiments that we use an algorithm to optimise. An input state, $|\psi\rangle_{\text{in}}$, is acted on by a series of operators, \hat{O}_i , before heralding measurements are performed to produce an output state, ρ_{out} .

the dominant noise sources (photon loss in the heralding measurements and in the final state) are included. Finally, using the BMSE for the problem of measuring a phase shift in an interferometer, we find states that beat both the optimal Gaussian state and the coherent state when the experiment operates with realistic prior knowledge and a reasonable number of experimental repetitions. This will enable experiments with current technology to create exotic states with enhanced phase-measuring capabilities.

I. OPTICAL QUANTUM STATE ENGINEERING

The quantum optics experiments we design follow the blueprint depicted in Fig. 2. In this scheme, we start with an N -mode state, $|\psi\rangle_{\text{in}}$, which consists of independent one- and two-mode states. This state is acted on by up to m operators in sequence, which each act on one or two modes, with the two-mode operations serving to mix and entangle the modes. Finally, in $N - 1$ of the output modes heralding measurements are performed, modelled by POVMs. When each of these heralding measurements are simultaneously successful, the state in the N^{th} mode is the output state, which we then apply our fitness function to. With appropriate choices of experimental elements (which we introduce below), many of the state engineering schemes in the literature fit into our blueprint illustrated in Fig. 2 [16–20].

Although N is flexible, here we concentrate on $N = 2$ modes because having more modes is more difficult for both experiments and for our computer simulations. Experimentally, having more modes requires more heralding measurements, which must all be successful, so typically this substantially lowers the overall probability for producing the desired output state. These measurements also tend to be one of the largest sources of noise in an experiment, so adding more modes increases the amount of noise present. And because the state space grows exponentially with the number of modes, exponentially more

States	Operations	Measurements
$ n\rangle$	$\hat{D}(\alpha)$	$ n\rangle\langle n $
$ \alpha\rangle$	$\hat{S}_i(\zeta)$	Bucket
$ \zeta\rangle_i$	$\hat{S}_{ij}(\zeta)$	Multiplex
$ \zeta\rangle_{ij}$	$\exp(i\hat{n}\phi)$ $\hat{U}_{ij}(T)$	$ x_\lambda\rangle\langle x_\lambda $

TABLE I. The states, operations and measurements that make up our toolbox of experimentally feasible elements. Here, i and j are arbitrary modes.

computing power is required to run simulations with additional modes. In the discussion section, we outline future work to overcome the computational challenges and enable $N > 2$ modes.

To design an experiment using the blueprint in Fig. 2, we need a toolbox of states, operations and measurements – the full list of these elements that we consider is given in Table I. Our focus is on producing experimental designs that are feasible with current technology, and hence our toolbox only contains such elements. Other elements can easily be added to this list, and the list can be customised to match the capabilities of a particular laboratory. Next, we introduce the states, operations and measurements in our toolbox. The reader already familiar with the theory behind the elements in the toolbox can skip ahead to the section *Using a genetic algorithm to design experiments*.

A. Number states and number measurements

The first input state we include is the number state, or Fock state, $|n\rangle$. Typically, an experiment would be restricted to number states of low n , as generating a state with a large number of photons is technically challenging, so we restrict our simulations to have at most $n = 5$ (though this can easily be modified). As an example, a single photon state can be produced using spontaneous parametric down-conversion [21–23]. In this process, a photon of a particular frequency may be spontaneously converted into two identical photons, each with half of the original frequency. A heralding measurement is then used to detect one photon in this pair, which signals the existence of the other (this can be extended for $n > 1$).

One of the most common measurements in optics is measuring the number of photons in a mode – *photon number resolving detection* (PNRD) – which is implemented with the POVM element $|n\rangle\langle n|$. However, it can be difficult to precisely measure the number of photons so we also include two more-easily-implementable measurements. The first of these is a *bucket detector* (aka *on/off*, *threshold*, or *click* detector). This measures whether at least one photon is absorbed by the detector (it ‘clicks’), but it is unable to determine the exact number of pho-

tons. It is represented by the POVM, $\{|0\rangle\langle 0|, \mathbb{I} - |0\rangle\langle 0|\}$, where \mathbb{I} is the identity. These are commonly found in laboratories, for example in the form of avalanche photodiodes [24].

If exact PNRDs are not available, an approximate photon number measurement can be implemented by using several bucket detectors in a *multiplex detector*. This is achieved by separating the mode you want to measure (the target mode) into several modes via spatial- or time-multiplexing. The former can be implemented via a series of beam splitters, as in [25], or by optical fibre splitters, as in [26]. The latter can be implemented using a series of interferometers with paths of varying length, as in [27]. A bucket detection is then performed on each of these separated modes. A perfect PNRD is obtained in the infinite limit of multiplexed bucket detectors, but otherwise there will be a non-zero probability that more than one photon enters the same bucket detector in a given run, resulting in uncertainty in the exact number of photons entering the detector.

We use the following POVM, from [26], to simulate this multiplex detection, which takes into account all possible coincidence detection patterns. Here, r is the number of bucket detection events and c is the actual number of photons in the target mode. The weights $w_r(c)$ are non-negative and satisfy $\sum_r w_r(c) = 1$. These rely on the number of bucket detectors, d , and on $S(c, r)$, which is the Stirling number of the second kind, which counts the number of ways of partitioning c objects into r non-empty subsets. More details on constructing this POVM are found in the Supplemental Material of [26], which uses methods from [28] to compute the weights. The POVM elements E_r are given by

$$E_r = \sum_{c \geq r} w_r(c) |c\rangle\langle c|, \quad w_r(c) = \frac{d! S(c, r)}{(d-r)! d^c}. \quad (1)$$

In our simulations we use a multiplex detector consisting of either five bucket detectors [25] or sixteen [26], but again this can be easily altered.

B. Coherent states and displacement operators

Coherent states are among the most readily available states as they are produced by a stabilised laser operating well above threshold [29]. To use them in our toolbox, we must construct them in the Fock basis. They can be defined by the action of the displacement operator on the vacuum, $|\alpha\rangle = \hat{D}(\alpha)|0\rangle$, where

$$\hat{D}(\alpha) = \exp(\alpha \hat{a}^\dagger - \alpha^* \hat{a}), \quad (2)$$

for $\alpha \in \mathbb{C}$, and where \hat{a} (\hat{a}^\dagger) is the annihilation (creation) operator. Alternatively, the following description of a coherent state in the Fock basis can be derived using the normally ordered form of the operator, described in [29]:

$$|\alpha\rangle = \exp(-|\alpha|^2/2) \sum_{n=0}^{\infty} \frac{\alpha^n}{\sqrt{n!}} |n\rangle. \quad (3)$$

In our simulation we have to truncate the Hilbert space, and therefore in order to simulate accurate states and operators we must limit the magnitude of $|\alpha|$; here we generally use a maximum value of $|\alpha| = 5$.

C. Squeezed states and squeezing operators

Squeezed states have a lower variance (in some quadrature) than coherent states, which makes them useful in a wide variety of applications, such as optical metrology [10]. The single mode squeezed vacuum state is defined by $|\zeta\rangle_i = \hat{S}_i(\zeta)|0\rangle_i$, where $\hat{S}_i(\zeta)$ is given by

$$\hat{S}_i(\zeta) = \exp \left[\frac{1}{2}(\zeta^* \hat{a}_i^2 - \zeta \hat{a}_i^{\dagger 2}) \right], \quad (4)$$

where $\zeta \in \mathbb{C}$ and \hat{a}_i^\dagger and \hat{a}_i are the creation and annihilation operators on mode i [29]. Similarly, the two mode squeezed vacuum state can be defined by $|\zeta\rangle_{ij} = \hat{S}_{ij}(\zeta)|0\rangle_i|0\rangle_j$, where $\hat{S}_{ij}(\zeta)$ is given by

$$\hat{S}_{ij}(\zeta) = \exp \left[\zeta^* \hat{a}_i \hat{a}_j - \zeta \hat{a}_i^\dagger \hat{a}_j^\dagger \right], \quad (5)$$

where, again, ζ is a complex number which defines the state. As with coherent states, the normally ordered forms of the squeezing operators give rise to a construction of the states in the Fock basis [29].

Both the single mode and the two mode squeezed vacuum states can be created by acting on the vacuum with non-linear optical elements, such as optical parametric oscillation or four-wave mixing. They are further related because the action of a beam splitter on a two mode squeezed state is to produce two single mode squeezed states [29].

Squeezed states are harder to generate than, for example, coherent states, but they are still feasible and are an important resource in many experiments, so we include these in our toolbox and in most of our runs of the algorithm. We also include squeezing operators in the toolbox, although we omit these from most of our runs, as implementing a squeezing operator on an arbitrary state is difficult and rarely available in laboratories, although it is possible [30].

D. Beam splitters and phase shifts

The phase shift operation is given by $\exp(i\hat{n}\phi)$, where $\hat{n} = \hat{a}^\dagger \hat{a}$ is the photon number operator. This is often straightforward to implement as a phase shift can be induced on a mode through changing the length of the optical path it has to travel, when compared to the other modes in the system, for example using a thermo-optic effect [31].

The beam splitter is a vital element of our toolbox as it allows interactions between the modes. They are also

readily available, and can be implemented by a partially reflecting mirror (e.g. a half-silvered mirror) or an interface between two glued-together glass prisms, among others [32]. The beam splitter operation is given by

$$\hat{U}_{ij} = \exp \left[\theta \left(\hat{a}_i \hat{a}_j^\dagger - \hat{a}_i^\dagger \hat{a}_j \right) \right], \quad (6)$$

where the probability of a photon being transmitted through the beam splitter is $T = \cos^2 \theta$ [33]. A ‘50:50’ beam splitter, which mixes the two input modes in equal superposition, refers to the case where $T = 0.5$.

E. Homodyne detection

To define homodyne detection we first require the generalised quadrature operator [29]:

$$\hat{x}_\lambda = \frac{1}{\sqrt{2}} \left[\hat{a} \exp(-i\lambda) + \hat{a}^\dagger \exp(i\lambda) \right], \quad (7)$$

where λ is the quadrature angle. Setting $\lambda = 0$ and $\lambda = \pi/2$ in the above expression gives the usual ‘position’ and ‘momentum’ quadrature operators, respectively. Homodyne detection is a projection onto the eigenstates of these quadrature operators. However, it is not possible to construct normalised eigenstates of the quadrature operators. Instead we construct states, $|x_\lambda\rangle$, defined by a complex number $x_\lambda = |x_\lambda| \exp i\lambda$, which obey the eigenvalue equation

$$\hat{x}_\lambda |x_\lambda\rangle = |x_\lambda| |x_\lambda\rangle. \quad (8)$$

These are not orthogonal but instead their overlap is given by the Dirac delta function

$$\langle x_\lambda | x'_\lambda \rangle = \delta(x_\lambda - x'_\lambda). \quad (9)$$

These eigenstates may also be constructed by operating on the vacuum state as follows [29]

$$|x_\lambda\rangle = \pi^{1/4} \exp \left[-\frac{1}{2}|x_\lambda|^2 + \sqrt{2}x_\lambda \hat{a}^\dagger - \frac{1}{2} \exp(2i\lambda) \hat{a}^{\dagger 2} \right] |0\rangle.$$

Perfect homodyne detection is the projection onto a single point in phase space, characterised by the projector $|x_\lambda\rangle\langle x_\lambda|$. Here, $|x_\lambda|$ and λ form the polar coordinates of the chosen point in phase space.

F. Simulating noisy experiments

The elements of the toolbox described so far assume the experiment to be noiseless at all stages: in preparing the initial state, in implementing the operations, in performing the heralding measurements and on the output state itself (although the multiplex and on/off detectors incorporate their intrinsic noise). However, realistic experiments will have sources of noise at each stage.

In modelling a realistic set-up, it is beneficial to include noise during the optimisation, as some optimised states are more robust to noise than others. So what is optimal in the ideal scenario may not be optimal in the noisy scenario. We therefore include the option to include noise in a given simulation.

We focus on the two most dominant noise sources in optics experiments taking the form of Fig. 2: i) imperfect photon detectors, which can be modelled as photon loss prior to detection, and ii) photon loss on the output state. Noise is also present in the initial state preparation and in implementing the operations, but we do not include these as they are typically smaller than the detection and output-state loss (though future work will also incorporate these).

Photon loss can be modelled by mixing the noisy mode with the vacuum using a beam splitter of transmissivity $T = 1 - \gamma$ (and hence loss rate γ) [33]. However, this is computationally expensive as it requires simulating an additional mode, so here we simulate loss using Kraus operators as follows [34]

$$\rho_{out} = \sum_{k=0}^{\infty} K_k |\psi_{in}\rangle \langle \psi_{in}| K_k^\dagger, \quad (10)$$

where ρ_{out} is the output state, $|\psi_{in}\rangle$ is the input state, and

$$K_k = \sum_{n=0}^{\infty} \sqrt{\binom{n}{k}} \sqrt{(1-\gamma)^{n-k} \gamma^k} |n-k\rangle \langle n|. \quad (11a)$$

The Kraus operator K_k represents the loss of k photons to the environment with loss rate of γ .

We can include loss in the measurements by modifying the POVM elements to [35, 36]

$$E_n = \sum_{k=n}^{\infty} \binom{k}{n} (1-\gamma)^n \gamma^{k-n} |k\rangle \langle k|. \quad (12)$$

For the bucket measurement, we use [36, 37]

$$E_0 = \sum_{n=0}^{\infty} \gamma^n |n\rangle \langle n|, \quad (13a)$$

$$E_1 = \mathbb{I} - E_0, \quad (13b)$$

where E_0 corresponds to a measurement of no photons and E_1 is the measurement of one or more photons. Finally, for the multiplex detector, we construct a set of POVMs by using Eq. (1) but with $|c\rangle \langle c|$ replaced with $E_{n=c}$ from Eq. (12).

II. USING A GENETIC ALGORITHM TO DESIGN EXPERIMENTS

To run our algorithm, the user first has to specify which input states, operators and measurements they

have available to them. This is done via a user interface (Fig. 9). As well as selecting the toolbox, the user can specify the ranges of the parameters, the loss rates of the detectors, the loss rate on the final state, and a number of other details.

Once a user has specified their toolbox, they next tell the algorithm what kind of final quantum state they require, by specifying a fitness function (more on this below). Next, we ask the question: *How can we best arrange the states, operators and measurements, so that the final quantum state maximises the fitness function?* This is a search problem; to perform this search, we use a genetic algorithm, which is a powerful and flexible global search metaheuristic based on evolution by natural selection. We describe some reasons for choosing a genetic algorithm in Appendix A.

Here we give a brief overview of our genetic algorithm; a more comprehensive description is given in Appendices B and C (also see [38]). First, we must encode each possible arrangement of states, operators and measurements into a vector, which is known as a *genome*. The genome contains all the information necessary to reconstruct a given experimental setup, including all the parameters of the elements in the experiment.

The genetic algorithm starts by creating a collection of genomes, which together are known as the *population*. Next, the experimental setup corresponding to each genome is simulated, and for each the fitness function is evaluated. The “fittest” genomes – i.e. the genomes with the largest fitness function – are then selected, and a new population of genomes is generated by mixing some of the genomes together (*crossover*) and by modifying (*mutating*) others. This next population should, in principle, be comprised of genomes that are “fitter”. This process repeats through a number of *generations*, until it is unlikely that any more generations will result in improvements. At this stage, if the algorithm has been designed appropriately, the fittest genomes will encode optimised solutions. Through this process, our genetic algorithm *evolves* quantum experiments that are highly suited to the task at hand. A flow chart of our algorithm is given in Fig. 3.

1. Optimising our algorithm for speed and efficiency

One of the most important considerations to make when running the algorithm is where to truncate the Hilbert space, i.e. the length of the vector representing a single mode state. Increasing this truncation increases the computational power required to run the algorithm, both in the time and memory, but truncating too low produces errors in the fitness function as not enough of the information about the state is included in its vector representation. To combat this, we allow the user to set a maximum truncation (see the user interface in Fig. 9). The fitness function will first simulate the circuit specified by the input genome at a very low truncation, then

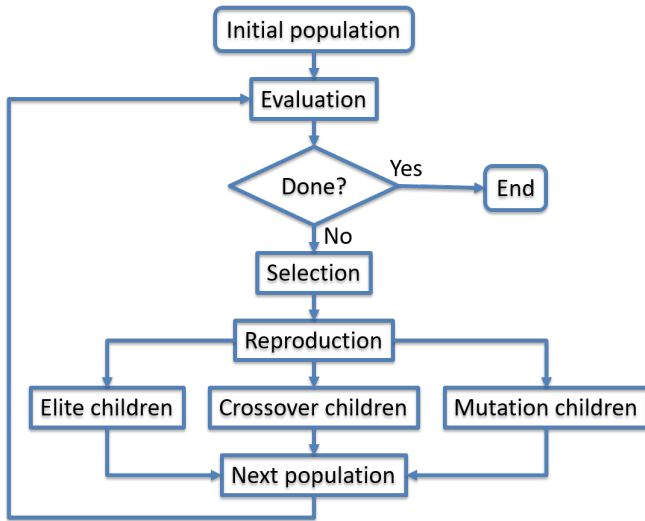


FIG. 3. Flowchart of a genetic algorithm – the various steps are described in the main text.

repeat this, increasing the truncation on each iteration, until either the average number of photons in the final state, \bar{n} , converges, or until the maximum truncation is reached. If \bar{n} has not converged at maximum truncation then the fitness function of the state is severely penalised.

To numerically simulate each quantum optics experiment, we must act a number of matrices (the operators) on the vector encoding the state, followed by a measurement operator and a partial trace of the measured modes. However, if this was implemented by just acting matrices on vectors, then, unless the truncation is small, the computation would be extremely slow (e.g. using Matlab, truncating at 30 photons typically allows simulations that run in the order of seconds on a standard desktop PC). But such small truncations are not nearly enough for the quantum states we wish to generate (see the results section). To overcome this we utilise Matlab's sparse matrix feature, and use analytical calculations to speed up a number of steps. But most importantly, we utilise the algorithm outlined in [39], and available as a Matlab function at [40], which speeds up implementing the operations by calculating $\exp(tA)b$ without needing to explicitly form $\exp(tA)$, where t is a scalar, A is a matrix and b is a vector. This produces a dramatic speed up, and allows us to simulate experiments with a truncation up to 170 photons in two modes in the order of seconds. This is significantly larger than comparable algorithms in the literature [1, 41]. As we will see next, this allows us to generate, among other things, quantum states comprised of a superposition of the vacuum with 80 photons.

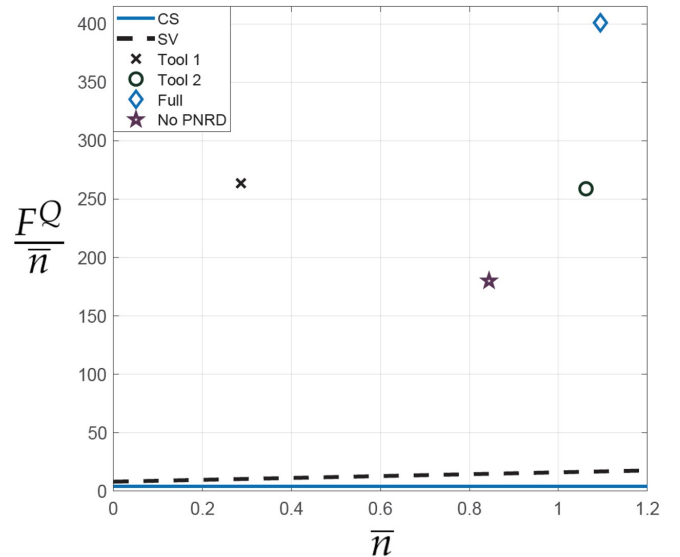


FIG. 4. Noiseless results: The QFI (for phase estimation), scaled by the average photon number, for each of the states produced by our algorithm, compared to the squeezed vacuum state (SV) and coherent state (CS). See Table. II for details of all the states. The toolboxes *Full*, *Tool 1*, *Tool 2*, and *No PNRD* are described in the main text. We see large improvements over the CS and SV, even for the experimentally-viable toolboxes *Tool 1*, *Tool 2*, and *No PNRD*.

III. RESULTS

In this section, we present the results of running the algorithm with several different fitness functions and toolboxes, which are all relevant to the field of quantum metrology.

A. Fitness function 1: Pure state QFI

For our first fitness function we consider only noise-free experiments, and we consider the quantum Fisher information (QFI) of the (pure) output state $|\psi\rangle$ for measuring an unknown phase ϕ . This is given by [9]

$$F^Q = 4(\langle\psi'_\phi|\psi'_\phi\rangle - |\langle\psi'_\phi|\psi_\phi\rangle|^2). \quad (14)$$

Here $|\psi_\phi\rangle = \exp(i\hat{n}\phi)|\psi\rangle$ is our state after the phase shift ϕ is applied, and $|\psi'\rangle \equiv \frac{\partial}{\partial\phi}|\psi\rangle$. The QFI is useful because it can tell us the precision with which our state $|\psi\rangle$ can measure the phase shift ϕ . This is found using the quantum Cramér-Rao bound (CRB) [9]:

$$\delta\phi \geq \frac{1}{\sqrt{\mu F^Q}}, \quad (15)$$

where $\delta\phi$ is said precision, and μ is the number of repetitions of the experiment. We see that the larger the QFI, the more precisely the phase can be measured, and hence we wish to find a state with a QFI as large as possible.

Note that $|\psi'_\phi\rangle = i\hat{n}|\psi_\phi\rangle$. We can therefore write Eq. (14) independently of ϕ , for example

$$|\langle\psi'_\phi|\psi_\phi\rangle|^2 = |\langle\psi_\phi|\hat{n}|\psi_\phi\rangle|^2 \quad (16)$$

$$= |\langle\psi|\hat{n}|\psi\rangle|^2 \quad (17)$$

In this way, we can calculate the QFI directly from the output state of our circuit, $|\psi\rangle$, without needing to perform any differentiation, which improves the performance of our algorithm.

The actual fitness function we use here is the QFI scaled by the average photon number of the output state, F^Q/\bar{n} . If we just used the un-scaled QFI, then the algorithm would just try to make bigger and bigger states, as even a classical state has an unbounded QFI in the large photon-number limit. Such an optimisation would soon produce states that require Hilbert-space truncations that are both too large to simulate, and require unrealistic experimental equipment. Using F^Q/\bar{n} overcomes this problem.

To judge the success of our results, we will compare the states we produce to a coherent state, which is the optimal *classical* state, and to a squeezed vacuum state, which is the optimal Gaussian state when there is no noise [42, 43].

Fig. 4 shows the results for the noiseless experiments found by AdaQuantum. Here, a different experimental scheme has been found for each of the four different toolboxes we have tested. The most expansive toolbox we studied is named ‘Full’ in the figure. This includes all of the toolbox elements listed in Table I (and described in Section I). Note that, for this toolbox, squeezing operators are allowed on arbitrary states. In this toolbox, the strength of the squeezing $|\zeta|$ is limited to 1.4 in both the squeezing operators and squeezed states; $|\alpha|$ is limited to 5 in both initial coherent states and displacement operators; and number states are limited to $n = 5$. The limit to the number of photons resolved by PNRDs is $n = 10$. The best experiment devised by the algorithm, detailed in Table II, utilises the squeezing operators and heralds on the detection of 10 photons. The resulting state has a F^Q/\bar{n} approximately 20 times higher than the corresponding squeezed vacuum state, and 100 times higher than the coherent state (and note that the squeezed vacuum state has a larger QFI than both the NOON state and the Holland and Burnett state [44–46]).

However, acting with squeezing operations on arbitrary states is extremely challenging at present, so we will move on to toolboxes ‘Tool 1’ and ‘Tool 2’. These are both the same as ‘Full’ but with the squeezing operations removed. They are very similar to each other, the only difference being that ‘Tool 2’ has the photon detection limited at $n = 10$, as in ‘Full’, and ‘Tool 1’ has the photon detection limited to $n = 6$. Running the algorithm with these toolboxes produced states with F^Q/\bar{n} still far higher than the squeezed vacuum and coherent state. Finally, we remove the ideal number measurements to form the toolbox ‘No PNRD’, which instead includes bucket

detectors and multiplex detection consisting of 16 bucket detectors, for up to 6 photon heralding. The resulting experiment found by Ada uses a heralding measurement on the vacuum $|0\rangle\langle 0|$ and produces a state with F^Q/\bar{n} still significantly higher than the squeezed vacuum. The states found by Ada for all these toolboxes are detailed in Table II, and schematics of a selection of the experiments designed by Ada are given in Fig. 5.

Why do these states give such large improvements over the alternatives? This can be revealed by looking at the number-distribution of the states. Here we focus on the state labelled ‘Tool 2’, and leave such an analysis of the other states for future work. By writing the state as

$$|\psi\rangle = \sum_{n=0}^{\infty} c_n |n\rangle, \quad (18)$$

in Fig. 6 we plot the log of $|c_n|^2$ against n . These coefficients were calculated both analytically and numerically. The figure reveals that this state has a large contribution of the vacuum, and a small but significant contribution of a huge number of photons, around 60-100. Such a state can be seen as a Schrödinger-cat-like state: the human eye can directly detect less than 100 photons [47], so, arguably, this state can be seen as a superposition of a macroscopic state with the vacuum. More importantly for metrology, such a state has a large QFI because it has a large variance, whilst retaining a small average number of photons. This state can therefore be seen as a realistic version of the so-called ON state, which has already attracted much attention in metrology [48, 49]. This state is also useful for quantum computing with continuous variables [50].

B. Fitness function 2: Mixed-state QFI

For our next fitness function, we study the effect of the two most dominant noise sources in the quantum optics experiments we are considering: photon loss at the output and imperfect heralding measurements. After this noise is applied the resulting state will be a mixed state ρ . We then apply the mixed-state QFI to this state (again scaled by the average photon number in the state, \bar{n}). To calculate the mixed-state QFI, we first need to apply the phase shift to ρ , giving ρ_ϕ , and then find the eigenvalues and eigenvectors of this state by writing it as $\rho_\phi = \sum_m q_m |\psi_m\rangle\langle\psi_m|$. We then use the form of the mixed-state QFI developed in [51]:

$$F^Q = \sum_i q_i F_i^Q - \sum_{i \neq j} \frac{8q_i q_j}{q_i + q_j} |\langle\psi'_i|\psi_j\rangle|^2 \quad (19)$$

where F_i^Q is the pure state QFI of eigenstate $|\psi_i\rangle$. We use a similar technique as with the pure-state QFI to write the mixed-state QFI so that it does not involve differentiation. It should be noted that we deal with pure states, in the form of vectors, until the measurement stage, when

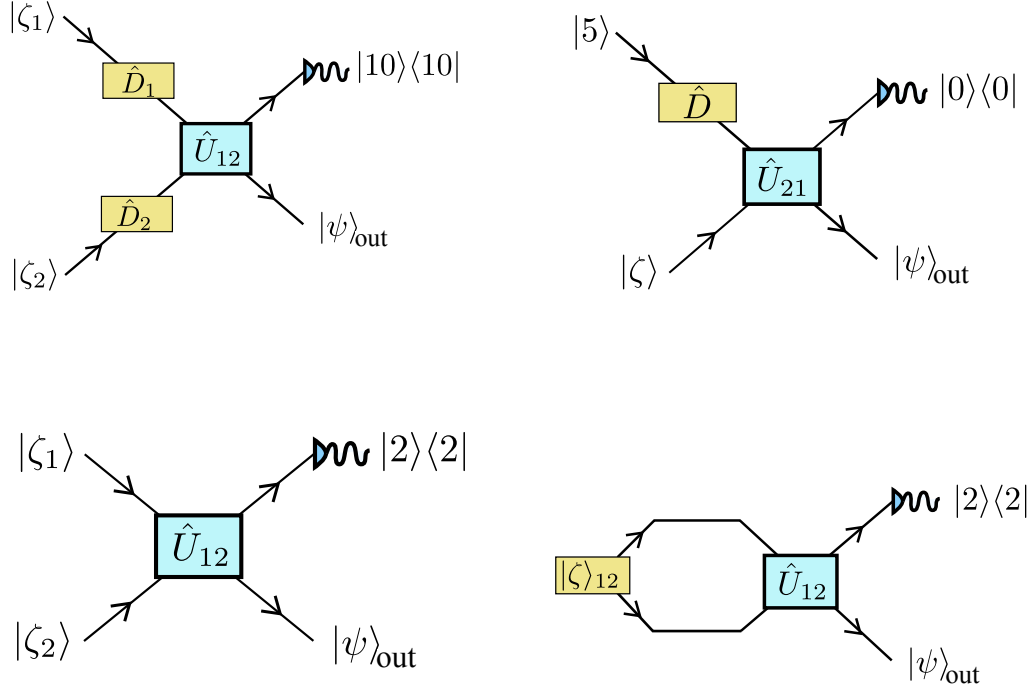


FIG. 5. A selection of the experiments designed by Ada. Top left and top right: These designs produce states that optimise the QFI, as introduced in Section III A. The performance of these states is shown in Fig. 4, and the details of the parameters are given in Table. II. The top left design uses the toolbox *Tool 1*, whereas top right uses toolbox *No PNRD*. Bottom left: A design to produce a state that optimises the QFI, after loss is applied to the measurement and final state, as introduced in Section III B. The performance of this state is shown in Fig. 7, where each loss rate requires different parameters. Bottom right: A design to produce a state that optimises the Bayesian mean square error (BMSE) with 1 repetition ($\mu = 1$), as introduced in Section III C. The performance of this state is shown in Fig. 8, and the details of the parameters are given in Table. IV.

Toolbox	ψ_{in}	\mathcal{O}_1	\mathcal{O}_2	\mathcal{O}_3	POVM	$p(\%)$
Tool 1	$ \zeta_1 = 1.39e^{i2.50}, \zeta_2 = 0.34e^{i5.64}\rangle$	$\hat{D}_2(\alpha = 2.49e^{i5.92})$	$\hat{D}_1(\alpha = 1.66e^{i6.11})$	$\hat{U}_{12}(T = 0.30)$	$ n = 10\rangle\langle n = 10 $	1.19
Tool 2	$ \zeta_1 = 1.40e^{i2.35}, \zeta_2 = 0.31e^{i5.44}\rangle$	$\hat{D}_2(\alpha = 1.97e^{i2.72})$	$\hat{D}_1(\alpha = 2.34e^{i5.98})$	$\hat{U}_{21}(T = 0.18)$	$ n = 6\rangle\langle n = 6 $	1.72
Full	$ 0, \zeta = 1.32e^{i0.06}\rangle$	$\hat{S}_{12}(\zeta = 0.88e^{i4.73})$	$\hat{D}_1(\alpha = 3.20e^{i6.28})$	$\hat{S}_2(\zeta = 0.19e^{i6.25})$	$ n = 10\rangle\langle n = 10 $	3.05
No PNRD	$ n = 5, \zeta = 1.40e^{i6.09}\rangle$	$\hat{D}_1(\alpha = 2.30e^{i4.62})$	$\hat{U}_{21}(T = 0.66)$	—	$ n = 0\rangle\langle n = 0 $	8.60

TABLE II. Toolboxes used and circuits produced for the results presented in Fig. 4 (schematics of a selection of the experiments designed by Ada are given in Fig. 5). The contents of each of the toolboxes are described in the text, and $p(\%)$ refers to the heralding success probability as a percentage. To clarify the notation used here, the state found with toolbox *Tool 1*, for example, is engineered by first creating a pair of squeezed vacuum states (with the parameters given in the table). Next, displacement operators act on both modes. A beam splitter is then applied, which entangles the two modes, and finally a 10 photon heralding measurement is performed. The probability of this heralding measurement being successful is 1.19%. The algorithm's flexibility means that we could easily re-run it to search for states with a higher heralding probability, if this was desired.

we switch to the density matrix formalism, as this allows us to use the matrix exponential technique discussed in section II 1 and in [39].

In the noiseless case, we saw that Ada found quantum states with dramatic improvements over the squeezed vacuum and coherent state. Noise will inevitably diminish such improvements, but up to now it has been an

open question whether it was possible to improve over the squeezed vacuum and coherent state *at all* when realistic experimental equipment and noise are factored in. Note that the squeezed vacuum and coherent state do not require heralding, so they escape the effects of imperfect heralding.

As discussed above, imperfect heralding can be mod-

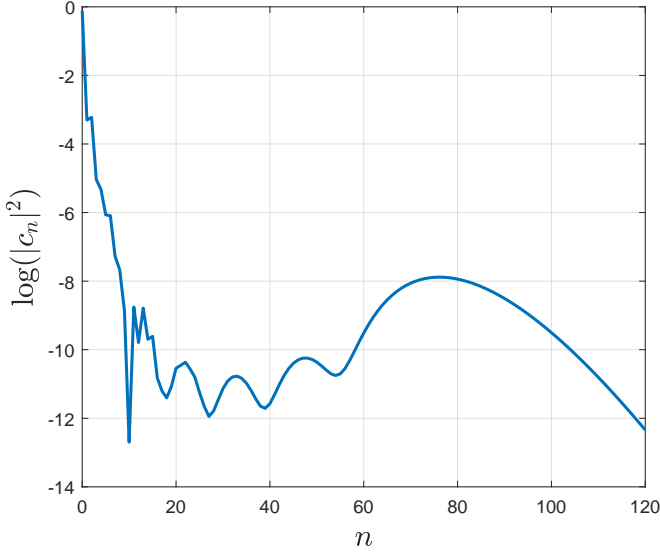


FIG. 6. Writing the state generated by ‘Tool 2’ as $|\psi\rangle = \sum_{n=0}^{\infty} c_n |n\rangle$, we plot the log of $|c_n|^2$ against n . We see that this state is a superposition of the vacuum with a large number of photons, and hence can be seen as a Schrödinger-cat-like state. To see how this state is made, see Table. II.

elled by applying loss to the state prior to heralding. For simplicity, we fix the loss to be the same for both the heralding measurements and on the output state. Unlike the noiseless case, here we are specifically focussed on experiments that can be realistically performed without specialised equipment. Therefore, the toolbox we use here does not use squeezing operations and has the following limits to the parameters: $n = 4$ for Fock states; $|\alpha| = 5$ for coherent states and displacement operator; $|\zeta| = 1$ for squeezed states; and photon number resolving up to $n = 6$.

The results produced for varying values of loss are shown in Fig. 7. The value of F^Q/\bar{n} for each of these results is higher than the squeezed vacuum at the same loss rate – this opens up the possibility for experiments using current technology to create these exotic non-Gaussian states, and use them to beat the squeezed vacuum state in phase estimation. The heralding probabilities to produce the desired output states are quite reasonable (around 10-20%) and so the experiments proposed here can be carried out experimentally in reasonable time.

C. Fitness function 3: Beyond the QFI

The third fitness function that we optimise here is the Bayesian mean square error (BMSE). Despite the importance of the QFI as a method of quantifying the metrological performance of different states, in general its usefulness depends on the possibility of recasting the problem at hand in the language of the local approach to estima-

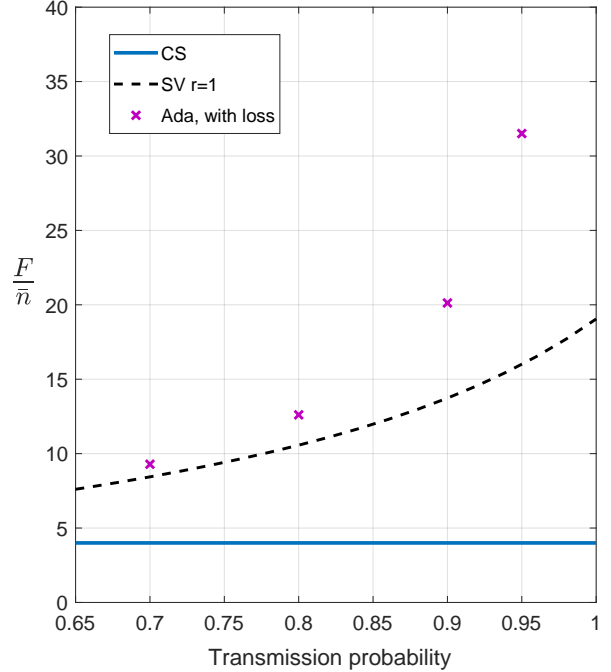


FIG. 7. We plot F^Q/\bar{n} of the states found by Ada against the transmission probability ($1 - \text{loss rate}$) of both the loss on the output state, and the loss in the heralding measurements. All states found by Ada take the form $|\psi\rangle = \mathcal{N}\langle 2|\hat{U}_{12}|\zeta_1, \zeta_2\rangle$, where \mathcal{N} is the normalisation, i.e. these states are formed by sending two squeezed vacuum states through a beam splitter, followed by 2-photon heralding. Note that, despite the fact that the states found by Ada have the same form for all loss rates, we optimised Ada for each loss rate separately. I.e. we first fixed the loss rate, then ran Ada to find states to maximise the QFI for that rate.

tion theory [11, 13–15, 52]. In particular, approaching the CRB in equation (15) typically requires either having certain prior knowledge and repeating the experiment a large amount of times [11, 12], or just having a large amount of prior information [13, 14]. But in realistic scenarios the number of repetitions of the experiment can be small, and the formalism based on the QFI does not take into account the possibility of having a moderate amount of prior information [15]. The BMSE factors in both of these, and hence gives a reliable measure of the phase-measuring capability of a given state in a realistic experimental setting.

To demonstrate what AdaQuantum can do using the Bayesian approach, suppose we prepare each of the two arms of an interferometer in the state $|\psi\rangle$, such that now a difference of phase shifts is encoded as $|\psi_\theta\rangle = \exp[-i(\hat{n}_1 - \hat{n}_2)\theta/2]|\psi\rangle \otimes |\psi\rangle$. Then a measurement is performed on both ports, which for simplicity we take to be ideal and given by the POVM elements $\{|M\rangle\langle M|\}$. The probability of finding the outcome M given the unknown value of the phase is $p(M|\theta) = \|\langle M|\psi_\theta\rangle\|^2$, and if the previous preparation and measurement stages are re-

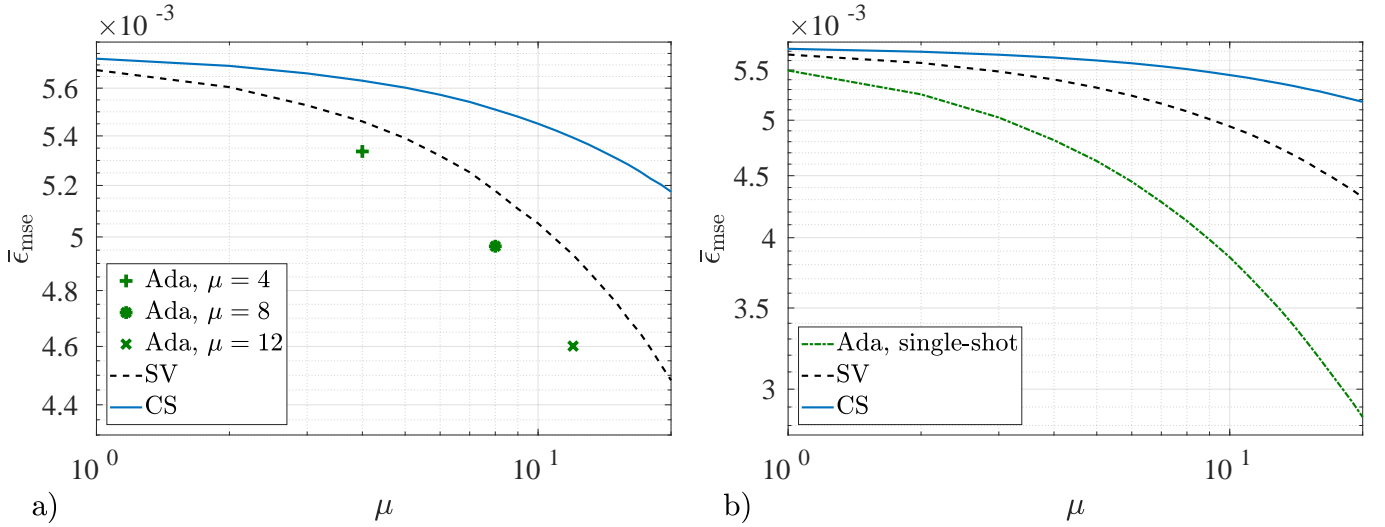


FIG. 8. Bayesian mean square error as a function of the number of repetitions for a) a coherent state mixed with the vacuum (solid line), two squeezed vacuums (dashed line) and states found by our genetic algorithm, Ada, for $\mu = 4$ (plus sign), $\mu = 8$ (asterisk) and $\mu = 12$ (cross) repetitions. Here the measurement scheme is based on counting photons after the action of a 50:50 beam splitter. In b) we again consider the coherent state and squeezed state, but now measured by their respective optimal single-shot POVMs. The state found by Ada (dash-dot line) is then based on the bound in equation (22), which already takes into account the optimal single-shot POVM for the given state. All the configurations are based on a two-mode interferometer with 1 photon on average, and where the phase shift can be found in an interval of width $\pi/12$, centred around zero.

peated μ times and the outcomes $\mathbf{M} = (M_1, \dots, M_\mu)$ are recorded, then their probability is $p(\mathbf{M}|\theta) = \prod_i p(M_i|\theta)$. Furthermore, imagine that we know in advance that the phase can only be found within an interval of width $\pi/12$ centred around zero, a state of knowledge that can be represented by the prior probability $p(\theta) = 12/\pi$, for $\theta \in [-\pi/24, \pi/24]$, and zero otherwise. We can then combine all these pieces of information using Bayes' theorem, which gives us the posterior probability $p(\theta|\mathbf{M}) = p(\theta)p(\mathbf{M}|\theta)/p(\mathbf{M})$, where $p(\mathbf{M})$ is the normalisation factor.

At this point we can introduce the BMSE as $\bar{\epsilon}_{\text{mse}} = \int d\mathbf{M} p(\mathbf{M}) \epsilon(\mathbf{M})$, where

$$\epsilon(\mathbf{M}) = \left\{ \int d\theta p(\theta|\mathbf{M}) \theta^2 - \left[\int d\theta p(\theta|\mathbf{M}) \theta \right]^2 \right\} \quad (20)$$

is the variance of the posterior probability. We note that since the posterior $p(\theta|\mathbf{M})$ contains the information about the phase, the BMSE can be understood as an optimal way of quantifying the quality of this information on average for a given POVM. In particular, $\bar{\epsilon}_{\text{mse}}$ is a measure of uncertainty. Further details and the justification of this framework can be found in [11, 13, 15, 53].

The task given to Ada is, in this case, to find single-mode states $|\psi\rangle$ that minimise $\bar{\epsilon}_{\text{mse}}$ for a given number of repetitions and measurement scheme. Since the calculation of the BMSE is more demanding than finding the QFI (see, e.g., [11]), we have chosen a narrow prior to simplify the calculation of the integrals in equation (20). However, this does not imply that we could have used the QFI instead, since it was argued in [15] that the

prior width needs to be 0.1 or smaller if the QFI is to be a suitable figure of merit in a similar scheme, and here the width is $\pi/12 \approx 0.3$. Thus our choice corresponds to the regime of intermediate prior knowledge where the BMSE is useful [15].

We will optimise the BMSE using two different strategies, both using the same toolbox as for the mixed-state QFI above. First we focus on a specific and practically-motivated POVM: counting photons after the action of a 50:50 beam splitter, and we set the algorithm to optimise the BMSE for $\mu = 4$, $\mu = 8$ and $\mu = 12$ repetitions. This search produces a state that takes the form $|\psi\rangle = \mathcal{N} \langle n | \hat{U}_{12} \hat{S}_{12} | 0, 0 \rangle$ for $\mu = 4$ and $\mu = 12$, where \mathcal{N} is the normalisation, while for $\mu = 8$ we find $|\psi\rangle = \mathcal{N} \langle n | \hat{P}_1 \hat{U}_{12} \hat{S}_{12} | 0, 0 \rangle$, where P_1 is a phase shift in the first mode. Table IV provides the numerical parameters that generate these states. The uncertainty associated with two copies of these probes for each number of trials has been represented in Fig. 8.a (individual points), and we have also included the BMSE of both an interferometer with a squeezed vacuum per port (dashed line) and the configuration that mixes a coherent state and the vacuum with a 50:50 beam splitter (solid line) [54]. This figure shows that the states found by Ada perform better than these two benchmarks, which constitutes a clear demonstration that Ada is able to optimise a Bayesian figure of merit beyond the regime where the QFI is useful.

More concretely, we can quantify this improvement by

Ada's relative enhancement					
50:50 beam splitter & photon counting				Single-shot POVM	
Ref.	$I_r(\mu = 4)$	$I_r(\mu = 8)$	$I_r(\mu = 12)$	Ref.	$I_r(\mu = 1)$
SV	0.02	0.04	0.07	SV	0.03
CS	0.05	0.10	0.15	CS	0.04

TABLE III. Improvement factor as defined in equation (21) to quantify the enhancement of the states found by AdaQuantum with respect to two squeezed vacuums (SV) and a coherent state mixed with the vacuum (CS). The details of the experimental configuration are those indicated in Fig. 8 and in the main text.

introducing the quantity

$$I_r = \frac{\bar{\epsilon}_r - \bar{\epsilon}_{\text{ada}}}{\bar{\epsilon}_r}, \quad (21)$$

where $\bar{\epsilon}_r$ is the BMSE of any of the two reference states that we are employing and a positive I_r indicates that there has been an improvement. Its calculation, whose results are summarised in table III, shows an enhancement of between 2% and 7% with respect to the squeezed vacuum, and between 5% and 15% with respect to the coherent state.

The second strategy is to perform an analytical optimisation over all possible POVMs first, and then set Ada to find experiments that optimise this strategy. (Note that during Ada's search, the optimal measurement scheme for estimating the parameters has been selected – Ada just optimises over the state-engineering part of the experiment, i.e. the arrangement of elements in Fig. 2). Following [15], first we recall that the single-shot BMSE satisfies [55–57]

$$\bar{\epsilon}_{\text{mse}}(\mu = 1) \geq \int d\theta p(\theta) \theta^2 - \text{Tr}(\bar{\rho} S), \quad (22)$$

where $S\rho + \rho S = 2\bar{\rho}$, $\rho = \int d\theta p(\theta) |\psi_\theta\rangle\langle\psi_\theta|$ and $\bar{\rho} = \int d\theta p(\theta) \theta |\psi_\theta\rangle\langle\psi_\theta|$. This bound can always be saturated when the measurement scheme is given by the projections onto the eigenstates of S [55–57], where S is an operator that only depends on the transformed state and the prior. Therefore, we can set the algorithm to search for states that minimise $\bar{\epsilon}_{\text{mse}}(\mu = 1, |M\rangle\langle M| = |s\rangle\langle s|)$, where $\{|s\rangle\}$ are the eigenvectors of S . Here we find another state with the form $|\psi\rangle = \mathcal{N}\langle n|\hat{U}_{12}\hat{S}_{12}|0,0\rangle$ but with different parameters (see table IV).

As table III shows, the state found by Ada for the optimal single-shot measurement is 3% better than two squeezed vacuums measured by their correspondent single-shot POVM, and 4% better than the coherent states. In addition, we note that using this measurement scheme in a sequence of repeated experiments is an appropriate strategy when we cannot or we do not wish to correlate different trials [15]. The performance of this state for the first 20 repetitions of the scheme, which has been represented in Fig. 8.b, shows that the state found by AdaQuantum using the optimal single-shot POVM

is better than the benchmarks even when the number of repetitions grows. To summarise, we can say that the combination of AdaQuantum and the methodology introduced in [15] provides a robust method to find practical probe states with a strong performance for those systems that operate in the regime of limited data.

IV. DISCUSSION

The results in the final section on the BMSE may have important general consequences for quantum metrology. The formal solution to the optimisation problem posed by a general quantum estimation scheme has been known for some time (see [56]). However, finding an analytical form of this solution for specific problems is challenging and generally not possible, which explains why we usually rely on bounds such as the CRB. And while in a sense the limits generated by the latter can be seen as fundamental [14], it can be argued that this is only useful when the bound can be safely applied to a problem in practice, which is not always the case (because realistic experiments put limits on the number of experiment repetitions and the prior knowledge available) [11, 12]. Therefore, the fact that our algorithm is able to find useful metrology protocols with more general fitting functions such as the BMSE or its single-shot optimum in equation (22) allows us to see it as a promising route to design quantum experiments using more reliable and general figures of merit, including, for instance, other cost functions different from the square error, or even multi-parameter systems [58, 59].

One clear direction for future work is to extend our runs of the algorithm to more than 2 optical modes. We attempted to do this in this project, but the additional simulation time required for > 2 optical modes meant that our global search was not effective. For 2 optical modes, most of the results presented here were generated by running the algorithm for 96 hours on 16 cores of the University of Nottingham's High Performance Computing facility. Running for such times allowed us to run the genetic algorithm with very large populations (in the order of thousands or tens of thousands). When moving to 3 modes, the exponential slow-down in computing time required to simulate this larger Hilbert space meant that such large populations were not possible. To overcome this, one main focus of our future work will be to significantly enhance the global search, by, among other things, exploring a range of metaheuristic search methods, and by improving the way the genome is encoded. We are confident that this will allow effective searches for quantum experiments in *at least* 3 modes, with the potential of finding quantum states with significant enhancements.

A further direction is to extend the fitness functions optimised by the algorithm. Ongoing work is searching for experiments to produce a range of specific states (such as squeezed cat states [60] and GKP states [7]). Beyond

Setting	ψ_{in}	\mathcal{O}_1	\mathcal{O}_2	\mathcal{O}_3	POVM
Ada, $\mu = 8$	$ 0, 0\rangle$	$\hat{S}_{12}(\zeta = 0.89 e^{i0.031})$	$\hat{U}_{12}(T = 0.69)$	$e^{i\hat{n}_1 0.32}$	$ n = 4\rangle\langle n = 4 $
Ada, $\mu = 4, 12$	$ 0, 0\rangle$	$\hat{S}_{12}(\zeta = 0.91 e^{i0.040})$	$\hat{U}_{12}(T = 0.66)$	—	$ n = 6\rangle\langle n = 6 $
Ada, $\mu = 1$	$ 0, 0\rangle$	$\hat{S}_{12}(\zeta = 0.95 e^{i6.1})$	$\hat{U}_{12}(T = 0.72)$	—	$ n = 2\rangle\langle n = 2 $

TABLE IV. Details of the circuits produced by AdaQuantum using the Bayesian framework. The first two are for a photon counting measurement after the beam splitter and that the last one is for the optimal single-shot POVM.

this, there are a broad range of fitness functions that could easily be incorporated, including searching for non-Gaussian states, highly entangled states, and states with a negative Wigner function. In time we aim to provide our algorithm open-access; but until then please get in contact if you would like to use and add to the algorithm, particularly with more fitness functions and additions to the toolbox.

In conclusion, we have introduced a genetic algorithm for designing quantum optics experiments. We demonstrated the flexibility of our algorithm by optimising three different fitness functions, and in all three the algorithm found improvements over the commonly used alternatives. Perhaps most notably, the algorithm found a realistic method of producing a Schrödinger-cat-like state comprised of a superposition of the vacuum with a large number of photons (around 80), which displays substantial phase-measuring improvements over the competing strategies. We emphasise here that our algorithm can in principle be used to design experiments to produce optical states with *any* desired properties, so long as these properties can be quantified and hence

optimised over. Our algorithm, together with related work in the literature [1–5], highlights the power of utilising methods from artificial intelligence and machine learning to design and optimise quantum experiments.

Acknowledgements: We thank Joseph Namara Hollis for the artwork in Fig 1. We acknowledge helpful discussions with Gerardo Adesso, Jacob Dunningham, Ryuji Takagi, and Ender Özcan. JR acknowledges support from the South East Physics Network (SEPnet). LM was supported by the Bristol Quantum Engineering Centre for Doctoral Training, EPSRC Grant No. EP/L015730/1. JCFM acknowledges support from an EPSRC Early Careers Fellowship (EP/M024385/1) and the EPSRC UK Quantum Technology Hub in Quantum Enhanced Imaging (EP/M01326X/1). PK acknowledges support from the Royal Commission for the Exhibition of 1851.

References

-
- [1] P. A. Knott, New J. Phys. **18**, 073033 (2016).
 - [2] M. Krenn, M. Malik, R. Fickler, R. Lapkiewicz, and A. Zeilinger, Phys. Rev. Lett. **116**, 090405 (2016).
 - [3] A. A. Melnikov, H. P. Nautrup, M. Krenn, V. Dunjko, M. Tiersch, A. Zeilinger, and H. J. Briegel, Proc. Natl. Acad. Sci. p. 201714936 (2018).
 - [4] J. M. Arrazola, T. R. Bromley, J. Izaac, C. R. Myers, K. Brádler, and N. Killoran, arXiv preprint arXiv:1807.10781 (2018).
 - [5] K. K. Sabapathy, H. Qi, J. Izaac, and C. Weedbrook, arXiv preprint arXiv:1809.04680 (2018).
 - [6] S.-Y. Lee, C.-W. Lee, H. Nha, and D. Kaszlikowski, JOSA B **32**, 1186 (2015).
 - [7] D. Gottesman, A. Kitaev, and J. Preskill, Phys. Rev. A **64**, 012310 (2001).
 - [8] Note1, the algorithm, AdaQuantum, is named after Ada Lovelace, the world’s first computer programmer, and resident of Nottingham, where our own algorithm was born.
 - [9] S. L. Braunstein and C. M. Caves, Phys. Rev. Lett. **72**, 3439 (1994).
 - [10] C. M. Caves, Phys. Rev. D **23**, 1693 (1981).
 - [11] J. Rubio, P. Knott, and J. Dunningham, J. Phys. Commun. **2**, 015027 (2018).
 - [12] D. W. Berry, M. J. W. Hall, M. Zwierz, and H. M. Wiseman, Phys. Rev. A **86**, 053813 (2012).
 - [13] R. Demkowicz-Dobrzański, M. Jarzyna, and J. Kołodyński, Progress in Optics **60**, 345 (2015).
 - [14] J. F. Haase, A. Smirne, J. Kołodyński, R. Demkowicz-Dobrzański, and S. F. Huelga, *Precision limits in quantum metrology with open quantum systems*, arXiv: 1807.11882 (2018).
 - [15] J. Rubio and J. Dunningham, *Quantum metrology in the presence of limited data*, arXiv: 1810.12857 (2018).
 - [16] T. Gerrits, S. Glancy, T. S. Clement, B. Calkins, A. E. Lita, A. J. Miller, A. L. Migdall, S. W. Nam, R. P. Mirin, and E. Knill, Phys. Rev. A **82**, 031802 (2010).
 - [17] T. J. Bartley, G. Donati, J. B. Spring, X.-M. Jin, M. Barbieri, A. Datta, B. J. Smith, and I. A. Walmsley, Phys. Rev. A **86**, 043820 (2012).
 - [18] A. Ourjoumtsev, H. Jeong, R. Tualle-Brouiri, and P. Grangier, Nature **448**, 784 (2007).
 - [19] K. Huang, H. Le Jeannic, J. Ruaudel, V. B. Verma, M. D. Shaw, F. Marsili, S. W. Nam, E. Wu, H. Zeng, Y.-C. Jeong, et al., Phys. Rev. Lett. **115**, 023602 (2015).
 - [20] J. Etesse, M. Bouillard, B. Kanseri, and R. Tualle-Brouiri, Phys. Rev. Lett. **114**, 193602 (2015).
 - [21] P. G. Kwiat, K. Mattle, H. Weinfurter, A. Zeilinger, A. V.

- Sergienko, and Y. Shih, Phys. Rev. Lett. **75**, 4337 (1995).
- [22] A. Lamas-Linares, J. C. Howell, and D. Bouwmeester, Nature **412**, 887 (2001).
- [23] C. Simon and D. Bouwmeester, Phys. Rev. Lett. **91**, 053601 (2003).
- [24] S. Cova, M. Ghioni, A. Lacaita, C. Samori, and F. Zappa, Appl. Opt. **35**, 1956 (1996).
- [25] G.-Y. Xiang, B. L. Higgins, D. Berry, H. M. Wiseman, and G. Pryde, Nature Photon. **5**, 43 (2011).
- [26] J. C. F. Matthews, X.-Q. Zhou, H. Cable, P. J. Shadbolt, D. J. Saunders, G. A. Durkin, G. J. Pryde, and J. L. O'Brien, npj Quantum Information **2**, 16023 (2016).
- [27] D. Achilles, C. Silberhorn, C. Sliwa, K. Banaszek, I. A. Walmsley, M. J. Fitch, B. C. Jacobs, T. B. Pittman, and J. D. Franson, J. Mod. Opt. **51**, 1499 (2004).
- [28] J. Sperling, W. Vogel, and G. S. Agarwal, Phys. Rev. A **85**, 023820 (2012).
- [29] S. M. Barnett and P. M. Radmore, *Methods in theoretical quantum optics*, vol. 15 (Oxford University Press, 2002).
- [30] Y. Miwa, J.-i. Yoshikawa, N. Iwata, M. Endo, P. Marek, R. Filip, P. van Loock, and A. Furusawa, Phys. Rev. Lett. **113**, 013601 (2014).
- [31] N. C. Harris, Y. Ma, J. Mower, T. Baehr-Jones, D. Englund, M. Hochberg, and C. Galland, Opt. Express **22**, 10487 (2014).
- [32] T. Inc., *Thorlabs online catalogue - optical beam splitters*, https://www.thorlabs.com/navigation.cfm?guide_id=18. Last accessed 2018-07-16.
- [33] P. A. Knott, Ph.D. thesis, University of Leeds (2015).
- [34] M. Nielsen, I. Chuang, and L. Grover, American J. Phys. **70**, 558 (2002).
- [35] M. O. Scully and W. E. Lamb, Jr, Phys. Rev. **179**, 368 (1969).
- [36] P. Kok, W. J. Munro, K. Nemoto, T. C. Ralph, J. P. Dowling, and G. J. Milburn, Rev. Mod. Phys. **79**, 135 (2007).
- [37] P. Kok and S. L. Braunstein, Phys. Rev. A **61**, 042304 (2000).
- [38] *Blog post with an introduction to genetic algorithms, using the medium of LEGO®*, <https://quantarei.wordpress.com/2018/08/08/using-a-genetic-algorithm-to-design-quantum-experiments/> (2018).
- [39] A. H. Al-Mohy and N. J. Higham, SIAM journal on scientific computing **33**, 488 (2011).
- [40] A. H. Al-Mohy and N. J. Higham, *expmv MATLAB code*, <https://github.com/higham/expmv>. Last accessed 2018-09-08.
- [41] N. Killoran, J. Izaac, N. Quesada, V. Bergholm, M. Amy, and C. Weedbrook, arXiv preprint arXiv:1804.03159 (2018).
- [42] A. Monras, Phys. Rev. A **73**, 033821 (2006), URL <https://link.aps.org/doi/10.1103/PhysRevA.73.033821>.
- [43] A. De Pasquale, P. Facchi, G. Florio, V. Giovannetti, K. Matsuoka, and K. Yuasa, Phys. Rev. A **92**, 042115 (2015).
- [44] J. Sahota and N. Quesada, Phys. Rev. A **91**, 013808 (2015).
- [45] H. Lee, P. Kok, and J. P. Dowling, J. Mod. Opt. **49**, 2325 (2002).
- [46] M. Holland and K. Burnett, Phys. Rev. Lett. **71**, 1355 (1993).
- [47] F. Rieke and D. A. Baylor, Rev. Mod. Phys. **70**, 1027 (1998).
- [48] A. Rivas and A. Luis, New J. Phys. **14**, 093052 (2012).
- [49] P. Knott, T. Proctor, A. Hayes, J. Ralph, P. Kok, and J. Dunningham, Phys. Rev. A **94**, 062312 (2016).
- [50] K. K. Sabapathy and C. Weedbrook, Phys. Rev. A **97**, 062315 (2018).
- [51] Y. M. Zhang, X. W. Li, W. Yang, and G. R. Jin, Phys. Rev. A **88**, 043832 (2013).
- [52] M. G. A. Paris, Int. J. Quant. Inf. **07**, 125 (2009).
- [53] E. T. Jaynes, *Probability Theory: The Logic of Science* (Cambridge University Press, 2003), ISBN 0521592712 hardback.
- [54] Note2, in [15] it was argued that if the prior probability is centred around zero and the POVM is based on mixing the light beams and counting photons, then for some probes it is necessary to also shift the phase of the second arm after the unknown parameter has been encoded in order to achieve the optimal BMSE. The calculations presented in this section have already taken this into account as prescribed by [15].
- [55] S. Personick, IEEE Transactions on Information Theory **17**, 240 (1971).
- [56] C. W. Helstrom, *Quantum Detection and Estimation Theory* (Academic Press, New York, 1976).
- [57] K. Macieszczak, M. Fraas, and R. Demkowicz-Dobrzański, New J. Phys. **16**, 113002 (2014).
- [58] P. C. Humphreys, M. Barbieri, A. Datta, and I. A. Walmsley, Phys. Rev. Lett. **111**, 070403 (2013).
- [59] T. J. Proctor, P. A. Knott, and J. A. Dunningham, Phys. Rev. Lett. **120**, 080501 (2018).
- [60] P. Knott, T. Proctor, A. Hayes, J. Cooling, and J. Dunningham, Phys. Rev. A **93**, 033859 (2016).
- [61] T. M. Inc., *Global optimization toolbox: User's guide (r2018a)*, <https://uk.mathworks.com/help/gads/index.html>. Last accessed 2018-07-17.
- [62] D. E. Goldberg, Goldberg.-[USA]: Addison-Wesley (1989).
- [63] A. R. Conn, N. I. M. Gould, and P. Toint, SIAM Journal on Numerical Analysis **28**, 545 (1991).
- [64] K. Deep and M. Thakur, Applied mathematics and Computation **193**, 211 (2007).
- [65] H. Barnum, H. J. Bernstein, and L. Spector, Journal of Physics A: Mathematical and General **33**, 8047 (2000).
- [66] G. Hornby, A. Globus, D. Linden, and J. Lohn, in *Space 2006* (American Institute of Aeronautics and Astronautics, 2006), p. 7242.
- [67] T. Geijtenbeek, M. Van De Panne, and A. F. Van Der Stappen, ACM Transactions on Graphics (TOG) **32**, 206 (2013).
- [68] B. Evans and S. P. Walton, Applied Mathematical Modelling **52**, 215 (2017).

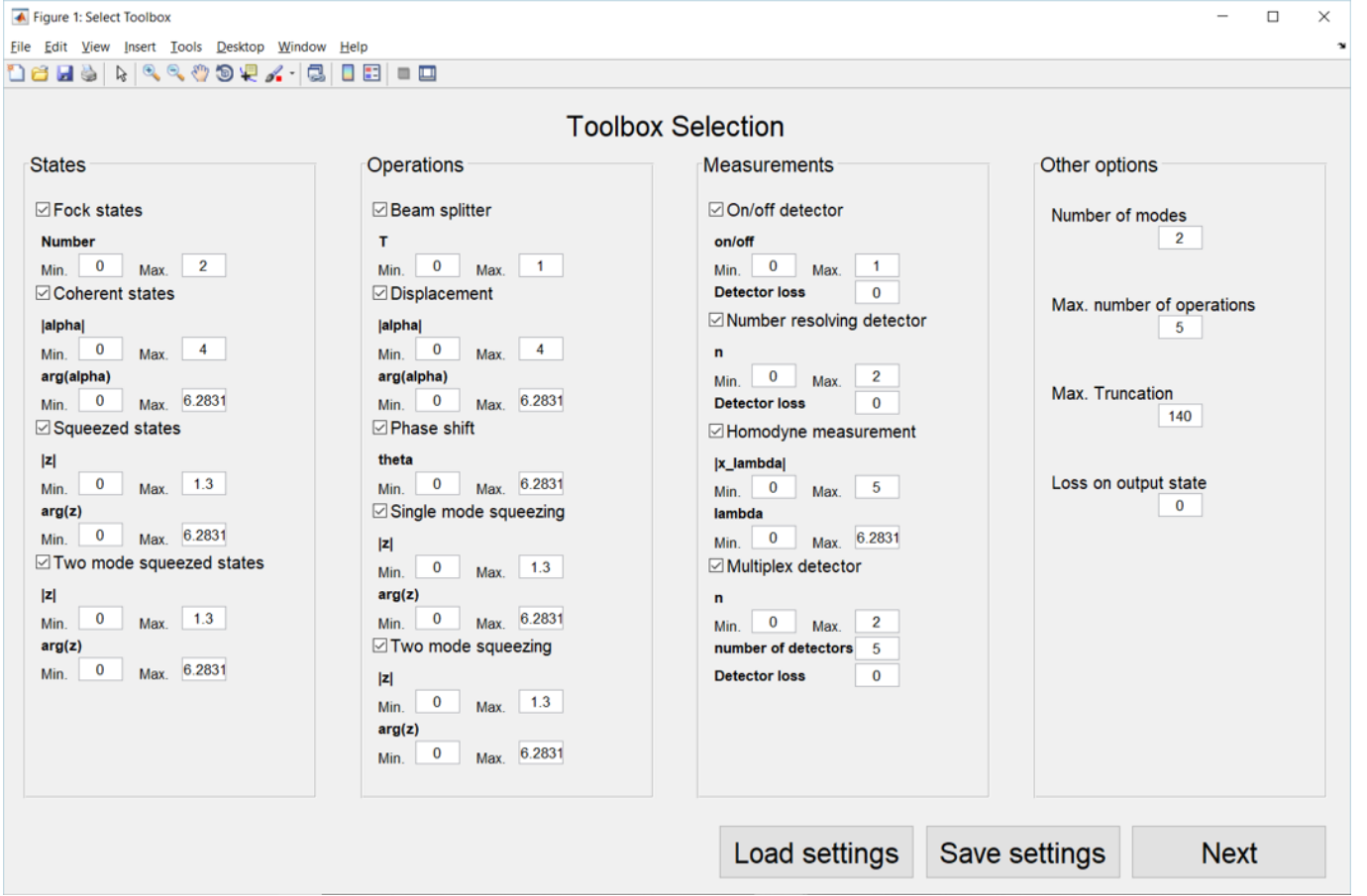


FIG. 9. The user interface that opens when first running our program, allowing the user to choose the elements of the toolbox they would like to optimise, and the limits on them. After pressing “Next”, the user is taken to a similar user interface that allows the fitness function to be specified. After this has been chosen the genetic algorithm runs and generates optimised experiment designs.

Appendix A: Why use a genetic algorithm?

To define a state preparation scheme, as in Fig. 2, a large number of variables are needed. Some of these, such as the magnitude of the displacement of a coherent state, $|\alpha|$, will be continuous and the value of the QFI of the output state will vary smoothly with these parameters. However, some others, such as the variable that chooses which type of input state to use for a particular mode, are discrete and the QFI of the output state will change in discrete, discontinuous jumps on the change of these variables. The gradient of the QFI with respect to these variables is also not well defined, and even for the continuous variables it is difficult to calculate. The large number of variables, the lack of a readily-calculable gradient, the discontinuous nature of the function space and the presence of many local minima makes the function challenging to optimise.

‘Hill climbing’ algorithms take an initial point in the space of the variables (chosen at random, or by the user if the approximate location of the optimum is known) and gradually improve the value of the figure of merit of that point by changing its position based on the gradient of the figure of merit at its current position. As we cannot calculate the gradient, these algorithms are inappropriate for our problem. Other techniques, such as pattern search, don’t use the gradient but may still be susceptible to getting stuck in local optima, and are therefore also not ideal either [61].

Genetic algorithms overcome these barriers as no gradient is required and they are effective at overcoming local optima. To do this, instead of varying a single point they vary a group of points known as the population and rather than using the gradient, the points are varied in techniques inspired by evolution: mutation and crossover. We therefore choose to use this algorithm to optimise our state engineering schemes.

Appendix B: Genetic algorithms

Genetic algorithms take inspiration from biological evolution [61–63]. The aim of the algorithm is to maximise (or minimise) the fitness function – a summary of how this is achieved is presented in Fig. 3. Before starting the algorithm, the fitness function must be defined. This is the function to be optimised, known as the objective function in standard optimisation algorithms, which must produce a real number (the *fitness* or *objective value*) from a collection of real variables. Any point that the fitness function can be applied to, i.e. a list of values for each of the variables, is known as a *genome*, and the individual values of variables in this genome are known as the genes.

The algorithm works by varying a group of points, known as the population. Hence, the first step is to generate the initial population. For each genome in the population, each variable is generated at random within the provided bounds. Then the algorithm must iterate the population, hoping to optimise the fitness function by finding genomes that improve on the best value of the fitness function of previous generations. This iteration has the following steps, which repeat until the stopping conditions are reached:

Evaluation: The value of the fitness function is found for each genome in the current population, these are known as the raw fitness scores. At this point the stopping conditions are also evaluated.

Selection: Using the results of the evaluation, a subset of the population known as the parents are selected.

Reproduction: The next generation is generated using the selected parents. This is done using three methods: elite, crossover and mutation.

The selection step works by first scaling the raw fitness scores to convert them into a more usable range of values. These scaled scores are then used to select the parents of the next generation. The selection function assigns a higher probability of selection to genomes with higher scaled fitness scores. This mimics natural selection, or ‘survival of the fittest’, as the ‘fitter’ genomes are more likely to reproduce.

The reproduction step creates genomes of the next generation (‘children’) using the parents of the current generation through three methods. The first are elite children, which form only a small percentage of the next generation. These are the parents with the highest fitness scores, which survive to the next generation unchanged. The second are crossover children. Here, two parents are chosen at random and each gene of the child is produced by copying the gene from one of the two parents, chosen at random. The final method to create children is mutation. Here, a single parent is chosen and random changes are made to its genome to produce the child (we created our own mutation function, based on [64], which is more flexible than Matlab’s built in mutation functions).

These children together form the next generation and the process repeats until the stopping conditions are met (see [38] for a visual introduction to genetic algorithms). Possible stopping conditions include meeting a maximum number of generations over which the best fitness score does not change, within tolerance. There is no proof that genetic algorithms must converge [61], but they have been known to perform well in situations where standard, gradient-based, optimisation algorithms have failed. In quantum circuit design, genetic algorithms have been successfully used to design quantum logic gates [65]. In other fields, examples of problems where genetic algorithms have been used include a NASA design of a radio antenna to pick up signals in space [66], computer models for walking for bipedal creatures [67] and optimising the aerodynamics of hypersonic space vehicles [68].

Appendix C: Our approach

Our genetic algorithm has three stages:

1. First, a large number of random genomes are created and evaluated. A collection of genomes with the best fitness values (FV; the fitness value is the number produced by the fitness function) are selected for the next stage. Due to the nature of the problem, many of the FVs are zero, so this stage rules out many of these zero FVs, and gives the genetic algorithm in the next stage a better starting population. In this stage the truncation of the Hilbert space is small (we vary this, but is often around 30), and therefore the quantum simulation is only approximate. But it is fast.
2. In the second stage, we run Matlab’s inbuilt genetic algorithm [61] with a medium-sized population. The simulation is less approximate than stage 1 (because the truncation is larger, around 80), and hence slower. This stage only runs for a set number of generations, usually 10. This stage performs a fast global search, and provides the final stage with a strong population.
3. In the final stage, the simulation is accurate but slow. In this stage, as described in the main text, the fitness function will first simulate the circuit specified by the input genome at a very low truncation, then repeat this,

increasing the truncation on each iteration, until either the average number of photons in the final state, \bar{n} , converges, or until the maximum truncation is reached (where the maximum truncation is specified by the user). This ensures the results are reliable and accurate, while still running in a reasonable time. Here the population is smaller, and the search is more local.

We compared our 3-stage genetic algorithm to Matlab's built-in pattern search, swarm, and simulated annealing algorithms. Our algorithm performed significantly better (though we didn't conduct a comprehensive comparison).
